Non-linear global pooling in the discrimination of circular and non-circular shapes

Gunnar Schmidtmann, Graeme J. Kennedy, Harry S. Orbach, Gunter Loffler *

Department of Vision Sciences, Glasgow Caledonian University, Cowcaddens Road, Glasgow, Scotland G4 0BA, UK

ARTICLE INFO

ABSTRACT

The ability to discriminate minute deviations from circularity is dependent upon global summation mechanisms integrating information along entire contours. The aim of this study was to determine how the strength of global summation depends on various stimulus features. To determine if the strength of global summation differs between shapes, contour discrimination for various contour shapes, generated by applying a sinusoidal modulation to the radius of a circle (radial frequency – RF – patterns), was measured. Shapes differed in frequency (number of lobes RF3, RF5 and RF20) and amplitude ('sharpness' of the lobes ranged between 0 and 20× thresholds for detecting deviation from a circle). Low amplitudes test discrimination against a circle while high amplitudes measure sensitivity for highly non-circular shapes (e.g. five-pointed star-shapes). The ability to integrate information along contours was assessed by comparing the effect of applying radial deformations to the entire contour or to only fractions (various number of cycles). Results show that discrimination thresholds remain in the hyperacuity range for low amplitudes, but increase for higher amplitudes. Concerning signal integration, discrimination, expressed as a function of the amount of contour deformed, exhibits a shallow and a steep regime. Discrimination improves only slowly as more contour cycles are deformed until the point when the entire pattern is modulated, when sensitivity increases substantially. The initial shallow regime is well captured by probability summation. The increase in sensitivity when the entire pattern is modulated compared to a single cycle provides evidence for global pooling. The pattern of integration and the existence of global pooling is dependent on shape frequency. The two-part behavior is independent of shape amplitude but is only seen for low RFs (3 and 5). Data for RF20 follow the prediction of probability summation.

We next investigated various stimulus characteristics and their effect on integration strength. Global pooling exceeding probability summation is evident for different pattern sizes, presentation times and for high as well as low absolute contrasts. Only if the contrasts of different fractions of a contour shape are individually scaled to match their respective visibilities is integration strength below the level of probability summation. This explains the lack of apparent global pooling in previous studies employing mixed contrasts.

The marked increase in performance for discriminating completely modulated RF patterns argues in favor of highly specialized, global shape mechanisms that are seen over a wide range of stimulus configurations. The results indicate global, non-linear mechanisms, which respond most strongly when stimulated by the entire pattern and comparatively weakly when only stimulated by parts of it.

© 2012 Elsevier Ltd. All rights reserved.

1. Introduction

The visual scene is composed of a vast variety of shapes and objects. Their retinal image is processed via a hierarchy of cortical areas starting with the primary visual cortex (V1), which contains simple line and edge detectors sensitive to orientation, spatial frequency, polarity and contrast (Hubel & Wiesel, 1962, 1968). At subsequent cortical stages (V2 and V4) along the ventral visual processing stream (Goodale & Milner, 1992; Ungerleider & Mishkin,

1982) detectors are selective for more complex stimulus features such as angles, arcs and circles (Anzai et al., 2007; Connor, Brincat, & Pasupathy, 2007; Dobbins, Zucker, & Cynader, 1987; Hegde & Van Essen, 2000; Pasupathy & Connor, 1999, 2001, 2002), as well as for hyperbolic and polar stimuli (Gallant, Braun, & Van Essen, 1993; Gallant et al., 1996). Finally, at higher cortical areas including IT and LOC, neurons have been shown to be selective for complex stimuli such as faces and whole objects (Goodale & Milner, 1992; Gross, 2008; Ito et al., 1994; Missal et al., 1999; Murray et al., 2002; Tanaka, 1996).

Object and shape perception inevitably requires the integration of local orientation information from early processing stages. How

---

 * Corresponding author. Fax: +44 1413313387.
   E-mail address: G.Loffler@gcu.ac.uk (G. Loffler).

this integration is achieved is as yet not completely understood (see Loffler, 2008 for a recent review).

Wilkinson, Wilson, and Habak (1998) investigated the properties of shape processing psychophysically using a class of closed contours known as radial frequency (RF) patterns. RF patterns are defined by sinusoidal modulations of a radius, where the frequency of the modulation determines the number of lobes (e.g. 5 vs. 8 sided shape) and the amplitude describes the sharpness of each lobe. Studies using fMRI (Dumoulin & Hess, 2007; Wilkinson et al., 2000) and ERP (Ohla et al., 2005) indicate that these kind of patterns are processed in human V4.

In their initial study, Wilkinson, Wilson, and Habak (1998) measured performance for discriminating RF patterns from circles. Thresholds were found to be in the 'hyperacuity' (Westheimer, 1979) range for patterns above RF2, as subjects were able to detect minute deviations (less than 10–15 arcsec) from circularity.

Theoretically, the discrimination between RF patterns and circular shapes could be realized by either local filters matched to parts of the pattern (e.g. points where the tangent or curvature of an RF pattern deviates the most from a circle) or by a global mechanism, using large filters and operating on the scale of the entire pattern, with access to information from the entire circumference of the shape. Wilkinson, Wilson, and Habak (1998) argued that subjects' remarkable sensitivity in RF discrimination tasks could neither be explained by local orientation deviation nor by local curvature analysis, but instead indicated global pooling of contour information. Further support for global strategies comes from a range of subsequent psychophysical studies (Bell & Badcock, 2008, 2009; Bell et al., 2007; Hess, Achtman, & Wang, 2001; Hess, Wang, & Dakin, 1999; Jeffrey, Wang, & Birch, 2002; Loffler, Wilson, & Wilkinson, 2003).

To describe the magnitude of global pooling, Loffler, Wilson, and Wilkinson (2003) measured the amount of pooling in a task of discriminating between various RF patterns and circles. Pooling was assessed by comparing sensitivity for variable amounts of contour deformation (number of modulated cycles). For some patterns, performance increased with the number of modulated cycles at a rate that exceeded the prediction of probability summation over multiple local independent detectors. This result supports the earlier proposal that a global mechanism underlies the high sensitivity seen in RF detection and allowed the global integration strength to be determined. However, global pooling was not found for all shapes tested. Global pooling was evident for low radial frequencies (RF3, RF5 and partially for RF10) but not for higher frequencies (RF24). It was suggested that the progressive change in the amount of summation is evidence that multiple shape mechanisms are responsible for processing these shapes (Loffler, Wilson, & Wilkinson, 2003). Studies using either adaptation (Anderson et al., 2007; Bell, Dickinson, & Badcock, 2008; Bell et al., 2009), sub-threshold summation (Bell & Badcock, 2009) or masking paradigms (Habak, Wilkinson, & Wilson, 2006; Habak et al., 2004) support the existence of multiple narrowly-tuned RF channels.

The main purpose of the current study was to examine the existence and strength of global pooling and to compare it across a range of factors including contour shape. The majority of previous studies have concentrated on discrimination between circular shapes and RF patterns (Bell & Badcock, 2008, 2009; Habak, Wilkinson, & Wilson, 2006; Hess, Wang, & Dakin, 1999; Jeffrey, Wang, & Birch, 2002; Loffler, Wilson, & Wilkinson, 2003; Wilkinson, Wilson, & Habak, 1998). Shapes tested in these studies only sampled quasi-circular shapes, which represent a restricted range of the multitude of possible closed contour shapes. Non-closed, sinusoidal contours have also been tested (Gheorghiu & Kingdom, 2009) as have non-circular RF patterns (Bell et al., 2009, 2010). For the latter case, supra-threshold (i.e. non-circular) RF patterns have been employed in adaptation (Bell et al., 2010)

and masking experiments (Bell et al., 2009), with evidence in favor of global processing of these shapes. What has not been done is to measure the integration strength for supra-threshold RFs and to compare this strength for circular and non-circular shapes. Note that in this paper the term *circular* describes RF contours close to discrimination thresholds against a circle (near-threshold) and *non-circular* refers to RF contours with high modulation amplitudes (supra-threshold).

As will be shown, a range of non-circular shapes are processed globally, similar to circular contours, but the integration process is highly non-linear and more complex than previously thought. Global integration is only evident when entire contours are modulated. When only a fraction of a shape is deformed, local processes are sufficient to explain experimental results.

The existence of global pooling underlying RF shape discrimination has recently been questioned for stimuli at low contrasts (Mullen, Beaudot, & Ivanov, 2011). In that study, sensitivity to a single, isolated cycle was found equal to that for the entire RF. The issue of global pooling has significant implications for the cortical mechanisms involved in contour shape processing as well as for models aimed at capturing their behavior. We therefore investigated the reasons for the differences between Mullen, Beaudot, and Ivanov's (2011) study and a range of other investigations (Bell & Badcock, 2008, 2009; Habak, Wilkinson, & Wilson, 2006; Hess, Wang, & Dakin, 1999; Jeffrey, Wang, & Birch, 2002; Loffler, Wilson, & Wilkinson, 2003; Wilkinson, Wilson, & Habak, 1998) by determining the circumstances under which global pooling is present.

2. Material and methods

2.1. Participants

Three of the authors, all experienced psychophysical observers, participated in all experiments. A further naïve subject completed a range of conditions to confirm the main results. All subjects had normal or corrected-to-normal visual acuity. The observations were made under binocular viewing conditions. No feedback was given either during practice or the experiments.

2.2. Apparatus

Stimuli were generated using Matlab 7.7 (Mathworks). The shapes were presented on a gamma-corrected LaCie "electron22blueII" monitor (1024 × 768) with a frame rate of 85 Hz under the control of a Macintosh G4 computer. The pattern luminance was on average 65 cd/m². Observers viewed the stimuli using a chin and forehead rest to guarantee a constant viewing distance of 120 cm. At this distance the size of 1 pixel was 0.018 deg. To avoid reference cues, a white cardboard mask with a circular aperture of 12 deg was placed in front of the monitor. Experiments were carried out under dim room illumination. Routines from the Psychophysics Toolbox were used to present the stimuli (Brainard, 1997; Pelli, 1997).

2.3. Stimuli

The radial frequency patterns used in the experiments are characterized by sinusoidal modulations of the radius of a circle according to the following equation (Wilkinson, Wilson, & Habak, 1998):

$$r(\theta) = r_{mean}[1 + A(\theta) \cdot \sin(\omega\theta + \varphi)] \tag{1}$$

where r (radius) and θ (polar angle) are the polar coordinates of the contour and r_{mean} is the radius of the modulated circle (corresponding

to the pattern size). A, ω and φ define the amplitude, radial frequency and phase (orientation) of the shape. The radial frequency determines the number of lobes in the pattern per 360 deg and the amplitude defines the sharpness of each lobe.

To enable individual cycles of a pattern to be manipulated independently from the remainder of the contour (Experiment 1), the amplitude, $A(\theta)$ is allowed to vary with polar angle. A smooth transition between successive cycles with different amplitudes was guaranteed by applying cumulative distribution functions to the amplitude, resulting in the following definition for $A(\theta)$:

$$A(\theta) = A_0 + \Delta A \cdot \left\{ \Phi\left(\frac{\theta + \theta_0 + \delta}{\sigma}\right) + 1 - \Phi\left(\frac{\theta - \theta_0 - \delta}{\sigma}\right) \right\} \qquad (2)$$

where A_0 and ΔA denote base and increment (relative to the base) amplitudes. θ_0 is the central point of the incremented region, which was always fixed at a zero-crossing of Eq. (1) and σ is the standard deviation, which defines the shape of the transitional region. The extent of the incremented region (δ) is set to be:

$$\delta = \frac{N}{2} \cdot \frac{2\pi}{\omega} \qquad (3)$$

where N ($N \leqslant \omega$) is the integer number of incremented cycles. $\Phi(x)$ is the cumulative distribution function of the standard normal distribution:

$$\Phi\left(\frac{x - \mu}{\sigma}\right) = \frac{1}{\sqrt{2\pi}} \int_{-\infty}^{x} e^{\frac{-(t-\mu)^2}{2\sigma^2}} dt = \frac{1}{2}\left[1 + erf\left(\frac{x - \mu}{\sigma\sqrt{2}}\right)\right] \qquad (4)$$

The last term (erf) refers to the error function. The function has a mean of μ and a variance of σ^2. The standard deviation (σ) of the cumulative distribution function, was defined as:

$$\sigma = \frac{\pi}{2\omega} \cdot \frac{\sqrt{2}}{erf^{-1}(2 \cdot prob - 1)} \qquad (5)$$

The first term specifies the extent of the transitional region (set to a quarter of a cycle in the experiments) and 'prob' determines its steepness. It was set to 0.965 so that the amplitude function reached 96.5% of the incremental amplitude within a quarter of a cycle.

When ΔA is zero, the resulting contour is an RF pattern with identical amplitude modulation throughout. We will refer to these shapes as 'pure' RFs (e.g. all patterns in the second row of Fig. 1 are pure RF5s with different amplitudes). In all experiments with complete RF contours, the reference pattern was always a pure RF while the increments had non-zero ΔA. The amplitudes of the reference patterns were set to multiples of the detection thresholds (discrimination of an RF against a circle). The actual incremented amplitudes depended on the condition and observer sensitivity. Incremented amplitude modulation was either applied to the entire contour (in which case both reference and increment were pure RFs) or to a fraction of the contour (see third row in Fig. 1, where an RF5 with a base amplitude (A_0) of 10× is presented with an incremental amplitude (ΔA) of 20× applied to 1, 2, 3, 4 or all 5 cycles).

In a second experiment, we measured sensitivity when individual cycles of contours were presented in isolation (with the remainder of the contour invisible). Discrimination thresholds were measured for such single RF cycles vs. circular arcs of the same angular extent. Individual cycles of an RF contour were isolated by manipulating the contrast of the contour along its circumference. The contrast of the contour for these conditions was determined by the following equation:

$$C(\theta) = \begin{cases} C_{nominal} \cdot e^{\frac{-(\theta - W/2)^2}{(sig/2)^2}}, & \theta > \theta + \frac{W}{2} \\ C_{nominal}, & \theta - \frac{W}{2} \leqslant \theta \leqslant \theta + \frac{W}{2} \\ C_{nominal} \cdot e^{\frac{-(\theta + W/2)^2}{(sig/2)^2}}, & \theta < \theta - \frac{W}{2} \end{cases} \qquad (6)$$

where C is the contrast as a function of polar angle (θ), $C_{nominal}$ is the desired contrast of the isolated cycle, sig is the space constant of the Gaussian (set to 15 deg) that was used to ramp down the contrast on either side of the isolated cycle and W determines the width of the window:

$$W = \frac{N \cdot 360}{\omega} \qquad (7)$$

N is the number of cycles (set to 1 in the experiments presented here) and ω the radial frequency of the RF pattern as above. Thus, the absolute angular size of the aperture depends on the radial
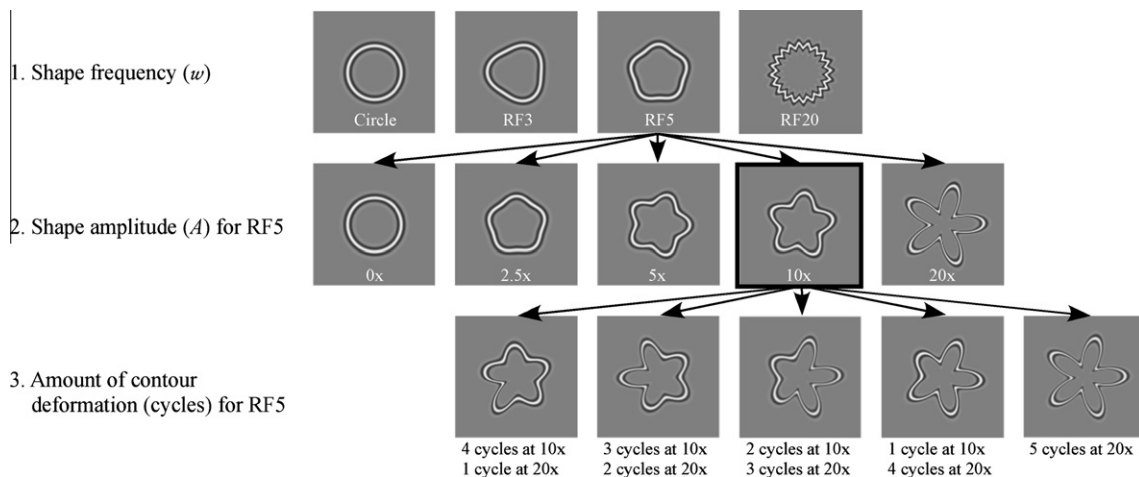

Fig. 1. Examples of contour shapes used in this study. Contours with various shape frequencies of RF0 (circle), RF3, RF5 and RF20 are shown in the first row. Discrimination ability was tested for reference shapes of different radial frequencies and amplitudes. RF3 and 5 were tested at several amplitudes (0×, 2.5×, 5×, 10× and 20× the amplitude at detection threshold of a given shape against a circle). RF20 was tested for 0×, 10× and 20×. The second row shows a range of amplitudes for an RF5. To assess the amount of global pooling, sensitivities for various amounts of contour deformation were compared. Thresholds were measured where the deformation added to the reference shape was restricted to within 1, 2 or all 3 cycles for an RF3; 1, 2, 3, 4 or 5 cycles of an RF5; 1, 7, 19 or 20 cycles of an RF20. The third row shows several test patterns for a reference shape of RF5 at 10× detection threshold (square with a black border in second row). The five patterns in the third row differ by the amount of contour (1–5 cycles) to which the deformation (20× in this example) has been applied; the remaining part of these contours have an amplitude of 10× (identical to the amplitude of the reference). Thresholds were defined as the amplitude of the deformed part (e.g. 20×) that had to be added to the test shape to be able to discriminate it from the reference (e.g. 10×).

frequency. The center of the window was always fixed to a zero-crossing of Eq. (1). Note that this approach guarantees an unattenuated part that extends over a full cycle at the desired contrast. The reference patterns were circular segments with the same angular extent (including Gaussian ramp) as the corresponding RF cycle.

The cross-sectional luminance profile of the stimuli was consistent with previous studies and characterized by a radial fourth derivative of a Gaussian (D4) (Wilkinson, Wilson, & Habak, 1998):

$$D4(r) = C\left(1 - 4\left(\frac{r - r_{mean}}{\sigma_{SF}}\right)^2 + \frac{4}{3}\left(\frac{r - r_{mean}}{\sigma_{SF}}\right)^4\right)e^{-((r-r_{mean})/\sigma_{SF})^2} \quad (8)$$

where C represents the contrast, r the radius in polar coordinates (Eq. (1)) and σ_{SF} defines the peak spatial frequency. For Experiment 1 the contrast was always set to the maximum (99%). In some of the conditions for Experiment 2, the contrast of the patterns was set to a multiple of individual observers' contrast detection thresholds. Contrast detection thresholds were measured for either a complete circle (setting $A = 0$ in Eq. (1)) or a circular arc with a size corresponding to a single cycle of the relevant RF pattern.

Stimuli were always presented with random orientations to exclude the subject's ability to predict the exact position of specific parts of the contour (e.g. points of maximum convex curvature at the corners, see Fig. 1).

2.4. Procedure

The method of constant stimuli with a temporal two-alternative forced choice paradigm was used. Observers were presented with two patterns, a test and a reference (see Fig. 1). Their task was to choose the contour (test), which had the higher amplitude (A; more modulated) by pressing one of two keys on a computer keyboard. The test and reference stimuli were randomly presented, so that the test stimuli could either be the first or second pattern. As an example, in one condition the black-bordered stimulus in row 2 of Fig. 1 (RF5 with 10× detection threshold) acts as the reference pattern and must be discriminated from the first stimulus in the third row of Fig. 1, where one cycle is modulated (with $A = 20×$ in this example). Each experiment consisted of six increments, which were selected based on the sensitivity of the observer with a logarithmic progression of the amplitudes of 2 db.

The monitor's background was initially set to a mean grey luminance. Each stimulus was then presented for 160 ms with an inter-stimulus-interval of 300 ms before the monitor returned to mid grey. The location of the patterns in all experiments was randomized within 7 pixels (0.124 deg) of the center of the screen. Each individual condition (e.g. RF3 vs. RF0) was tested within one block. Each of the six increments was presented 30 times within a block, giving a total number of 180 repetitions per threshold estimate for each experimental condition.

Firstly, detection thresholds (discrimination between a circle and an RF pattern) were measured for the three frequencies (RF3, RF5, RF20). These thresholds are referred to as baseline thresholds (0×). For RF3 and RF5 the individual baseline thresholds were then multiplied by 2.5, 5, 10 and 20, respectively, to measure increment thresholds for a range of different shapes (e.g. discriminating five-pointed star-shapes; see row 2 in Fig. 1). To investigate higher radial frequencies, thresholds for an RF20 were obtained for 10× and 20× the baseline threshold.

To assess the existence and the extent of global summation for a range of shapes, sensitivities were compared when deformation was restricted to various fractions of the contour. Thresholds were measured where the deformation added to the reference shape was restricted to within 1, 2 or all 3 cycles for an RF3; 1–5 cycles of an RF5; 1, 7, 19 or 20 cycles of an RF20. The third row in Fig. 1 shows several test patterns for a reference shape of an RF5 at

10× detection threshold (pattern with a black border in second row). The five patterns in the third row differ by the amount of contour to which the deformation has been applied (1–5 cycles); the amplitude of the deformed part is 20× in the figure.

Data, percent correct responses as a function of deformation amplitude, were individually fitted by a Quick function (Quick, 1974) using a maximum likelihood procedure. Detection thresholds were defined as the modulation amplitude yielding 75% correct responses. Observers usually completed three experimental runs for each experimental condition and their results were averaged.

3. Experiments

3.1. Experiment 1: Strength of global pooling for circular and non-circular shapes

The contrast of all stimuli in Experiment 1 was set to the maximum (99%), the size of the patterns (r_{mean}) to 0.5 deg, the cross-sectional profile had a peak spatial frequency of 8 cpd and the presentation time was 160 ms.

At first, baseline thresholds (0× detection thresholds) for discriminating entirely modulated (pure) RF3 and RF5 against a circle were individually measured for each observer. The results are given by the rightmost data points in the top parts of the diagrams in Figs. 2 and 3 (part 'A') for RFs of 3 and 5 respectively. To assess the strength of integration, discrimination thresholds between circles and RF patterns with contour deformation restricted to various fractions of the contour were determined. The abscissa in all plots shows the number of modulated cycles and the ordinate represents the thresholds expressed as Weber fractions, which are defined as the ratio between the modulation amplitude at threshold and the mean radius of the pattern (A/r_{mean}).

In order to test sensitivity for a range of non-circular shapes, we subsequently measured discrimination thresholds for several amplitudes, which were set at multiples (2.5×, 5×, 10× and 20×) of the individual baseline detection thresholds measured in the first part of the experiment. The absolute amplitudes were therefore different for different observers. The data for RF3 and RF5 with increasing amplitudes are shown from top to bottom (A–E) in Figs. 2 and 3. The icons on the right side of each plot illustrate the respective reference stimulus.

Thresholds are always lowest for discriminating an RF pattern from a circle (Figs. 2 and 3, part 'A'). Thresholds also decrease with increasing number of deformed cycles (left to right in each plot in Figs. 2 and 3). Differences between conditions for each RF were assessed with a repeated measure ANOVA with shape amplitude and number of modulated cycles as factors. The main effect of amplitude is significant (RF3: $F(4,8) = 6.47$, $p = 0.013$; RF5: $F(4,8) = 32.4$, $p < 0.001$). Post hoc tests (LSD) showed significant differences (increase in thresholds) between 2.5× and 5× ($p = 0.04$) and 2.5× and 10× ($p = 0.016$), respectively for RF3. For RF5 the increase in thresholds with increasing amplitude was statistically significant between 0× and 20× ($p = 0.007$), between 2.5× and 5× ($p = 0.033$), between 2.5× and 20× ($p = 0.024$), between 5× and 20× ($p = 0.023$) and between 10× and 20× ($p = 0.002$). This confirms earlier reports (Bell et al., 2009) and shows that a star-shaped pattern is harder to discriminate from a (somewhat) less pointed star-shaped pattern, than a rounded pentagon is from a circle.

Previous investigations have shown that subjects are remarkably sensitive for RF discrimination against a circle (Wilkinson, Wilson, & Habak, 1998), with thresholds falling in the hyperacuity range (for frequencies above RF2). For RFs with r_{mean} of 0.5 deg the hyperacuity range of between 10 and 15 s of arc (Westheimer, 1979) corresponds to Weber fractions of 0.0056–0.0083. Our
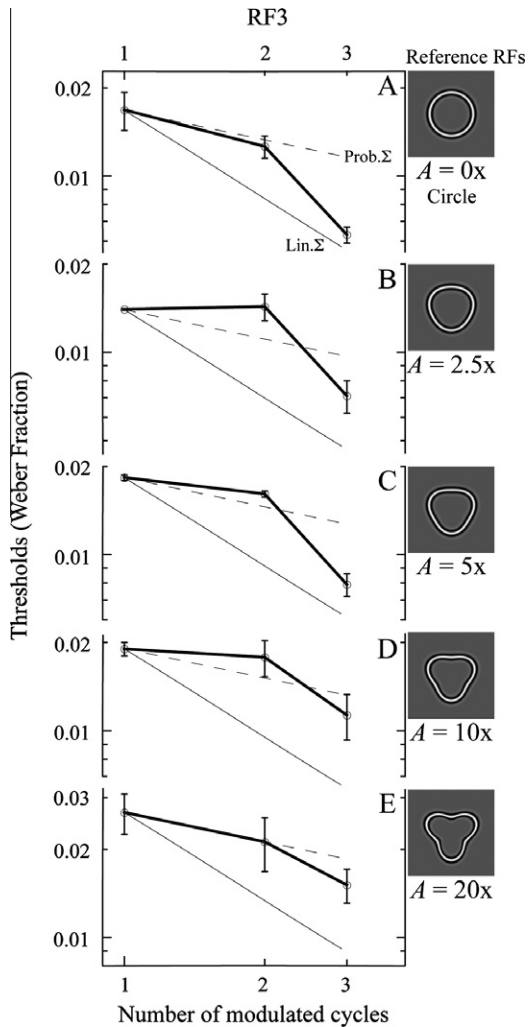
Fig. 2. Dependence of modulation discrimination threshold (ordinate) on the number of cycles (abscissa) for an RF3 for five different amplitudes (A–E). Thresholds are defined as the ratio between the modulation amplitude and the mean radius of the contour (A/r_{mean}) and these Weber fractions are plotted on log–log coordinates. The icons on the right side of the plots represent the reference patterns. The top graph shows the baseline ($0\times$) discrimination task, where subjects had to discriminate an RF3 with 1, 2 or all 3 cycles modulated against a circle. The amplitudes of the reference patterns in conditions B–E are multiples of the baseline threshold ($2.5\times$, $5\times$, $10\times$ and $20\times$) set individually for each observer. Data are the means over three observers. Error bars represent the standard errors of the means. Thresholds increase with increasing modulation amplitude (A–E). For fully modulated contours (rightmost data point in all plots), thresholds for patterns with amplitudes up to $2.5\times$ fall in the hyperacuity range (0.0056–0.0083). Discrimination thresholds decrease with increasing number of modulated cycles (left to right). Perfect linear pooling (Lin. Σ) would result in a slope of −1, indicated by the thin lines in the graphs. Probability summation (Prob. Σ) over multiple independent detectors would predict a slope of −0.33 indicated by the dashed lines. Data for an RF3 do not follow either of these predictions. Rather than following a simple power-law relationship (linear dependence in log–log coordinates), data show a moderate increase in performance from 1 to 2 cycles, which is in the range of probability summation and a dramatic increase in performance for pure RF3 patterns (3 cycles) resulting in a kink (see text and Fig. 4 for explanations). One naïve observer completed this experiment at $0\times$ and $5\times$ detection thresholds for 1–3 cycles (data not shown) and his data showed the same dependence of thresholds on number of cycles as the other observers.

results show that thresholds for discriminating *pure* RFs up to and including modulation amplitudes of $2.5\times$ for RF3, $5\times$ for RF5 and $10\times$ for RF20 fall in this range.

There was also a significant main effect of the number of modulated cycles for both RFs: RF3: $F(2,4) = 41$, $p = 0.002$; RF5: $F(4,8) = 16.83$, $p = 0.001$. Comparing performance (Fisher's least
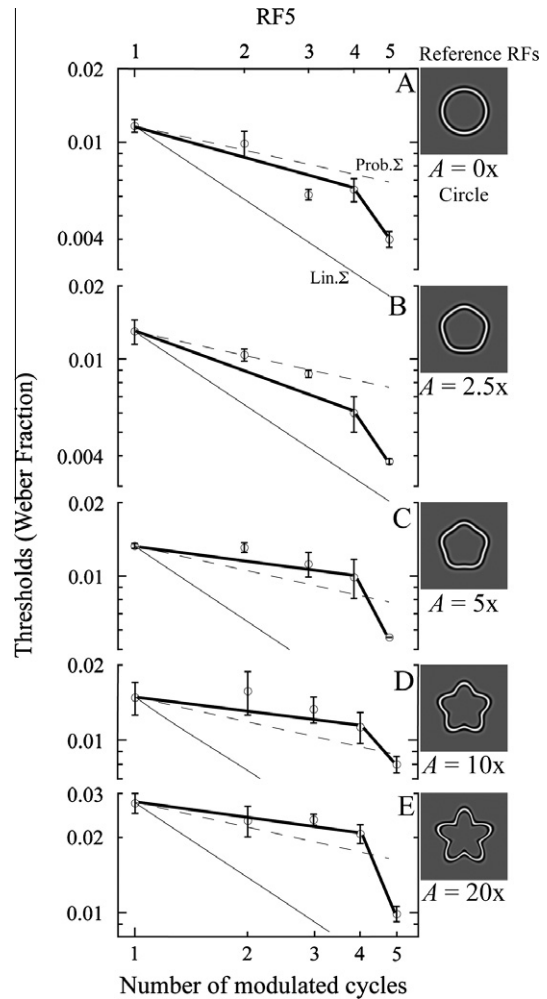
Fig. 3. Dependence of modulation discrimination threshold on the number of modulated cycles for an RF5 pattern with various amplitudes (A–E). Thresholds were measured for 1–5 cycles of an RF5 pattern (left to right in each plot). Thresholds increase with increasing modulation amplitude (A–E). For fully modulated contours, thresholds up to $5\times$ the baseline threshold fall within the hyperacuity range. Similar to RF3 patterns (Fig. 2), data for RF5 consistently show only a slight increase in sensitivity until a critical point (4 cycles for an RF5). Sensitivity improves dramatically when all 5 cycles are modulated. Hence, the data are not well captured by a simple power-law relationship. The increase in performance for the shallow part is well described by probability summation. (See text and Fig. 4 for further discussion.) The black lines connect performance for 1 with 4 cycles (shallow part) and 4 with 5 cycles (steep part) respectively. One naïve observer completed this experiment at $0\times$ and $5\times$ detection thresholds for 1–5 cycles (data not shown) and his data showed the same dependence of thresholds on number of cycles as the other observers.

significant difference (LSD) post hoc tests) for a pure RF with that when only fractions were modulated showed statistically significantly differences between 1 and 3 cycles ($p = 0.021$) and between 2 and 3 cycles for an RF3 ($p = 0.022$). For an RF5 this analysis revealed differences between 1 and 5 cycles ($p = 0.006$), between 2 and 5 cycles ($p = 0.037$) and between 3 and 5 cycles ($p = 0.015$).

RF discrimination could be determined by either individual local detectors or by a global integration process, pooling information along the entire circumference of the shape. If information was processed by independent detectors on a local basis, one might think that performance should be unaffected by the number of modulated cycles. This is too simplistic a prediction and a more appropriate one would be to take into account that sensitivity should improve even with independent detectors, each of which is affected by its own noise. The increase in performance as more
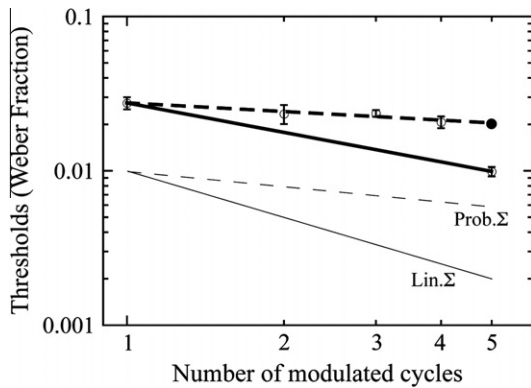
Fig. 4. Determining integration strength. First, to determine if a two-line fit is more applicable than a single-line fit and therefore assess the presence of a non-linear relationship between thresholds and number of modulated cycles, the slope of the shallow part (in the case shown here of an RF5 spanning from 1 to 4 cycles) was used to predict the performance when the entire pattern was modulated (5 cycles). The extension of the shallow part is indicated by the dashed line and the predicted performance for 5 cycles (pure RF5) is shown by the filled circle. Confidence intervals (95%) for the measured discrimination thresholds for this point were calculated (error bars for all data points represent 95% confidence interval) and compared with the prediction. The prediction is outside the confidence interval confirming the presence of a dramatic improvement in sensitivity from 4 to 5 modulated cycles. The predictions for both of the low frequencies (RF3 and 5) and all amplitudes tested were consistently above the 95% confidence interval, i.e. performance was always better than that predicted by a single power-law dependence. This argues in favor of a two-line fit being more appropriate to describe the data. The thin line, comparing one modulated cycle to when the entire contour is modulated (5 cycles) is a measure of the strength of global pooling. The slopes of these lines are considerably higher than probability summation but less than ideal linear summation (Lin. Σ), which would result in a slope of −1.0 (thin line). Average slopes for global pooling are: RF3 = −0.65; RF5 = −0.61.

and more of the contour is modulated would be predicted by probability summation over independent detectors (Graham & Robson, 1987; Loffler, Wilson, & Wilkinson, 2003). Local, independent detectors could, for example, be tuned to the contour's orientation (Mullen, Beaudot, & Ivanov, 2011), or its curvature (Dobbins et al., 1987; Dobbins, Zucker, & Cynader, 1989; Koenderink & Richards, 1988; Wilson, 1985; Wilson & Richards, 1989). Probability summation would predict a power-law function (i.e. linear relationship in log–log coordinates) between thresholds and the number of modulated cycles with a slope of −0.33 (Graham & Robson, 1987; Loffler, Wilson, & Wilkinson, 2003). This value is based on the average slope of the psychometric functions, which has been shown to be in the region of 3 (Graham & Robson, 1987) for these types of RF discrimination experiments (Bell & Badcock, 2008; Hess, Wang, & Dakin, 1999; Loffler, Wilson, & Wilkinson, 2003). The inverse of the average slope of the psychometric functions leads to the specific prediction of threshold improvement with cycles. The dashed lines in the graphs of Figs. 2 and 3 represent this prediction of probability summation (Prob. Σ). If, on the other hand, signals of multiple local detectors were more efficiently combined, performance should increase more dramatically with the extent of contour being deformed. Ideal global pooling mechanisms would predict a slope of −1 in log–log coordinates. This efficient pooling mechanism is referred to as ideal or linear pooling (Graham, 1989). The prediction of linear summation (Lin. Σ) is shown by the thin continuous lines in the graphs in Figs. 2 and 3.

Contrary to either of the two predictions (probability summation or linear pooling), the observed dependence of thresholds on the number of deformed cycles is not linear in log–log coordinates and therefore does not follow a power law relationship. Rather, the data for RFs 3 and 5 show a 'knee-shaped' characteristic, which is similar across various amplitudes (A–E). The graphs consistently show a shallow part extending from 1 to 2 cycles for RF3 and 1
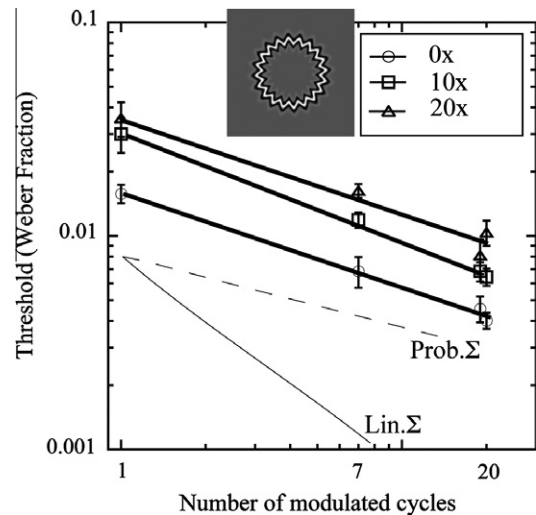

Fig. 5. Dependence of discrimination on the number of modulated cycles for an RF20 for three different amplitudes. To investigate discrimination thresholds for a high RF pattern, data for a RF20 were measured for 1, 7, 19 and 20 modulated cycles. Thresholds were determined against a circle (open circles, baseline) and for 10× (squares) and 20× (triangles) the baseline threshold. Performance decreases with increasing amplitude. For fully modulated contours, thresholds up to 10× the baseline threshold fall in the hyperacuity range. Thresholds also decrease with the number of modulated cycles. However, in contrast to low RFs (RF3 Fig. 2 and RF5 Fig. 3) the improvement in performance with increasing number of cycles is completely described by a single power-law fit with slopes (average = −0.4) in the range of probability summation (dashed line).

to 4 cycles for RF5 and a dramatic decrease (steep part) from 2 to 3 cycles for RF3 and 4 to 5 cycles for RF5. Subjects are substantially better at discriminating patterns when the entire contour changes than discriminating patterns where most but not all of the contour is modulated.

To confirm the existence of the non-linear ('knee-shape') relationship, we carried out the following analysis, in which thresholds for entire modulated contours are compared to those predicted by the shallow part (1–2 cycles for RF3 and 1–4 cycles for RF5). Prediction of performance for pure RFs (i.e. 3 cycles of RF3 and 5 cycles of RF5) was based on extrapolating the slopes of the best fitting line (power-law relationship) through the data points for 1 and 2 cycles of an RF3 and through 1–4 cycles of an RF5 (dashed line in Fig. 4). The filled circle in Fig. 4 represents the predicted performance for one condition (RF5 5×). Confidence intervals (95%) were then calculated for the measured thresholds and those were compared to the predictions. For both shapes and all amplitudes, the predictions underestimate sensitivity and fall outside the 95% confidence interval. This argues in favor of a two-line fit being more appropriate to describe the data.

The average slopes extending from 1 to 2 cycles (RF3) and 1 to 4 cycles (RF5) are in the range of probability summation (−0.20 for RF3 and −0.32 for RF5). There are several ways to describe the slopes of the steeper part. We decided to compare thresholds for a single modulated cycle with those when the entire contour is modulated (see Fig. 4) to describe the extent of global pooling. The improvement in performance (expressed as the slope of the line connecting these points in log–log coordinates) yields average slopes that are considerably steeper (RF3 = −0.65; RF5 = −0.61) than those predicted by probability summation (−0.33) but lower than linear pooling (−1.0). This cannot be explained by local mechanisms. Instead, it is evidence for a process that sums information globally but less efficiently than a linear integrator. This is consistent with reports by Loffler, Wilson, and Wilkinson (2003) on RF and similar sub-linear pooling characteristics have also been

observed in studies investigating the detection of Glass patterns (Wilson & Wilkinson, 1998).

These estimates of integration strength are in broad agreement with previous reports by Loffler, Wilson, and Wilkinson (2003). For an RF5, Loffler et al. found a slope of −0.69, which is remarkably consistent with the data presented here. However, for an RF3 they reported a steeper slope (−0.86 vs. −0.65). This is likely a consequence of the former study determining the slope by comparing performance for 1/2 cycle with that for the entire contour (3 cycles) while we used 1 and 3 cycles in the current study. As has been shown recently for low contrast RFs (Mullen, Beaudot, & Ivanov, 2011), performance improves drastically for fractions of a contour up to about 1 cycle. Hence, using fractions of a cycle to determine the overall integration slope may result in an overestimation of the amount of global pooling.

To investigate whether the non-linear characteristic ('knee-shape') is also evident for higher RFs, an RF20 was tested at three different amplitudes: at 0×, 10× and 20× the baseline threshold (Fig. 5). On the basis of the dramatic increase in performance from 2 to 3 and 4 to 5 cycles evident for RF3 and 5 respectively, thresholds for RF20 patterns were determined for 1, 7, 19 and 20 cycles (pure RF20).

As for the lower RFs, performance for RF20 decreases with increasing modulation amplitude. Moreover, data for RF20 also show an increase in performance with increasing number of cycles. However, in contrast to RF3 and RF5, the non-linear behavior with respect to the extent of modulated contour is not evident for an RF20. Rather, the data are well fit by a straight line indicating a simple power-law relationship between threshold and deformed area. The slope of the fit is on average −0.4 and thus in the range of probability summation. Together, these data suggest global pooling for low RFs (3 and 5) but not for high RFs (20). The non-linear behavior for low RFs indicates that global summation requires that the entire contour has to be deformed.

3.2. Experiment 2: Factors affecting integration strength

Recently, Mullen, Beaudot, and Ivanov (2011) measured discrimination thresholds at low contrasts for single RF cycles (displayed in isolation) against circular arcs, which were then compared with thresholds for entire, pure RF contours. In contrast to previous reports (Bell & Badcock, 2008, 2009; Habak, Wilkinson, & Wilson, 2006; Hess, Wang, & Dakin, 1999; Jeffrey, Wang, & Birch, 2002; Loffler, Wilson, & Wilkinson, 2003; Wilkinson, Wilson, & Habak, 1998), no significant difference in discrimination ability for single cycles vs. entire RFs was found. This led the authors to raise doubts about global strategies in this type of contour shape processing (Mullen, Beaudot, & Ivanov, 2011).

To investigate these discrepancies, we first considered the fact that single RF cycles were presented in isolation in their study, whereas they were part of an otherwise un-modulated contour in our experiments. We therefore determined thresholds for single isolated RF cycles and compared them to the thresholds when 1 cycle is modulated with the rest of the RF remaining circular (left-most data point in Figs. 2A and 3A). In addition to RF3 and 5, we ran this experiment with two further shapes (RF4 and RF8), one of which (RF4) was used by Mullen, Beaudot, and Ivanov (2011). Data for an RF5 are shown in Fig. 6A.

For the case of an RF5 as shown in Fig. 6A, subjects performed best for a pure, fully modulated RF (right hand data point in Fig. 6A). Discrimination thresholds for single modulated cycles within an otherwise circular contour (open circle on left hand side) are considerably higher (data replotted from Fig. 3). Importantly, thresholds for single cycles of a closed contour are similar to those for isolated cycles (filled squares). Differences were analyzed with a repeated measures ANOVA with the cycle conditions (i.e.

complete RF, single RF cycle and isolated RF cycle) as factors. This revealed a significant main effect ($F(2,4) = 29.9$, $p = 0.004$). Post hoc tests (LSD) comparing performance between one modulated cycle with the otherwise circular contour and the single isolated cycle were not significant ($p = 0.52$) but both conditions differed from a pure RF (entire contour modulated; $p < 0.05$). Data for the other shapes (RF3, RF4 and RF8) are not shown but they followed the same pattern of results with significant differences between each of the two single cycle conditions and an entirely modulated RF.

In all plots of Fig. 6, we define the strength of global signal integration as the slope of the line, which connects the threshold for a single modulated cycle presented in isolation to that for an entirely modulated RF (apart from Fig. 6A, which also shows the integration slope based on a single modulated cycle as part of an otherwise circular contour). As before, probability summation would predict a slope of −0.33. The prediction of linear global pooling in experiments with isolated cycles depends on the assumptions of the limiting noise and can differ from that when a single cycle is modulated as part of an otherwise un-modulated contour. Assuming early noise, increasing the number of visible cycles increases the number of early stage units integrated by a global integrator while increasing the amount of contour modulation does not affect the number of integrated units. Assuming noisy input units, the slope in the former case (noise and signal both increase) would be −0.5, while in the latter case (only signal increases with constant noise) it would be −1.0 (Morrone, Burr, & Vaina, 1995). Fig. 6 shows the predictions for perfect linear summation in the case of isolated cycles as −0.5. The reader is referred to the Discussion (Section 4.2) for further details regarding this issue.

The slopes for isolated cycles are −0.87, −0.41, −0.61 and −0.34 for RF3, 4, 5 and 8, respectively. The corresponding slopes for partially modulated patterns are similar: −0.89, −0.53, −0.67 and −0.52. Given that these slopes are in excess of probability summation, this confirms that global summation is evident irrespective of the way in which a fraction of a RF contour is isolated. Consequently, this cannot account for the lack of global processing reported in Mullen, Beaudot, and Ivanov's (2011) study.

In addition to employing isolated cycles, the stimuli and experimental parameters in the Mullen, Beaudot, and Ivanov (2011) study differed from ours in a number of other ways. Mullen et al. used larger stimuli with typically lower cross-sectional spatial frequencies, different shape frequencies, longer presentation times, lower contrast, employed a different algorithm to extract single cycles of an RF contour, used a staircase procedure and provided auditory feedback. It seems that the most likely factors responsible for the reported differences would be the shape of the patterns, stimulus size (in combination with spatial frequency), the presentation time, contrast and the details of the window used to isolated cycles. We investigated each of these.

Firstly, the typical size ($r_{mean} = 2.4$ deg), spatial frequency (SF = 1.5 cpd) and shape (RF 4) used in the earlier study differed from the stimuli here ($r_{mean} = 0.5$ deg; SF = 8 cpd, RF 5). As can be seen from our data in Fig. 6B, discrimination thresholds for single isolated cycles and complete RFs for different shapes (RF4 and 5), sizes and contour spatial frequencies follow a similar pattern. Although overall thresholds are higher for smaller patterns, global summation is evident for small RF5 contours with high spatial frequencies (slope = −0.61) as well as large RF4 contours with lower spatial frequencies (slope = −0.46). Note that this extends the results of a previous finding (Wilkinson, Wilson, & Habak, 1998) that RF discrimination is scale invariant. Although the two patterns are not exactly scaled (the choice was forced by the different patterns used in experiments presented here and those in Mullen, Beaudot, and Ivanov (2011)), these results suggest that the amount and nature of the integration strength is largely independent of scale. Hence, neither scale nor RF shape can account for the lack of global
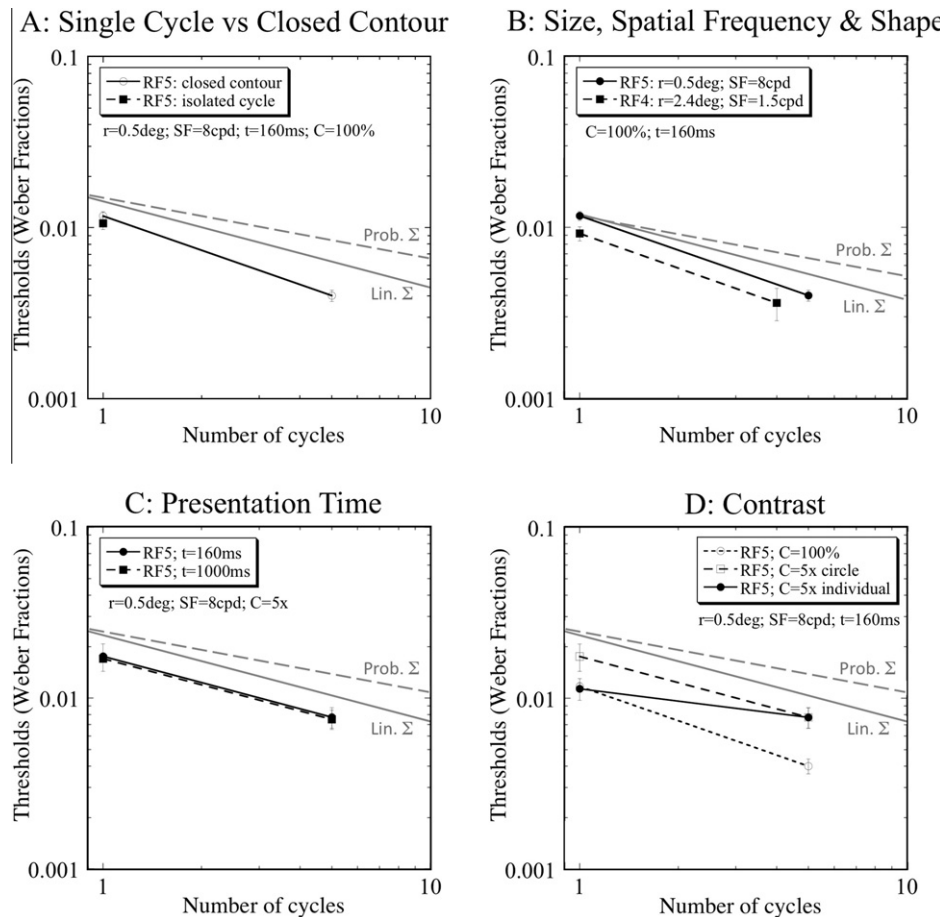
Fig. 6. Factors affecting integration strength. (A) Effect of isolating fractions of a contour, (B) effect of shape (RF), size (r_{mean}) and contour spatial frequency (SF), (C) effect of presentation time and (D) effect of contrast. In all plots, the strength of global signal integration is defined as the slope of the line which connects the threshold for a single isolated cycle (apart from (A), where data are also shown for a single modulated cycle as part of an otherwise circular contour) to that for an entirely modulated RF (4 or 5 cycles for RF4 and 5, respectively). The dashed grey lines indicate the prediction of probability summation (Prob. Σ) and the solid grey lines that of linear summation (Lin. Σ) with a slope of -0.5 (see text for further explanation). (A) Thresholds for single cycles of a closed contour (open symbols) are similar to those for isolated cycles (filled squares), hence the slopes are similar too. The slope connecting a single isolated cycle and the completely modulated RF is -0.61 compared to -0.67 for partially modulated contours. (B) Thresholds are higher for a small RF5 ($r = 0.5$ deg) with contour spatial frequency of 8 cpd compared to a larger RF4 ($r = 2.4$ deg) with spatial frequency of 1.5 cpd. Differences in threshold are similar for isolated cycles and fully modulated contours. Consequently, the slopes (-0.61 and -0.46) for the different conditions are similar and both in excess of probability summation. This suggests that for low RFs the strength of global pooling is largely independent of scale and pattern shape. (C) Presentation time (160 ms vs. 1000 ms) has no significant effect on thresholds tested with an RF5 pattern with $r = 0.5$ deg and contour spatial frequency of 8 cpd. The visibility of the patterns was matched in this condition and the contrasts set to five times the respective contrast detection thresholds for circles presented for short and long presentation times. The resulting slopes are -0.50 and both exceed the prediction of Prob. Σ. (D) For an RF5 with $r = 0.5$ deg and spatial frequency of 8 cpd, lowering the contrast from 100% (open circles, replotted from (B)) to five times the contrast detection threshold (CDT), of a circle (open squares, replotted from (C)) decreases sensitivity for isolated cycles and entire contours by similar amounts (the two black dashed lines are vertically shifted relative to each other and almost parallel). The strength of integration is similar (-0.61 for 100% contrast; -0.51 for 5$\times$ CDT). Hence, global pooling is seen for high and low contrasts. However, when the visibility of each stimulus is matched to its own contrast detection threshold (filled circles), the resulting data fall on a line that is much shallower. These data were collected with different absolute contrasts: single isolated cycles and full contours were presented at 5$\times$ their respective CDT, which results in higher absolute contrast values for the single cycle than the full contour. As a consequence, the slopes (i.e. integration strength) decrease because the contrast for the single cycle is higher (and thereby yielding a lower shape discrimination threshold) than that for the entire contour. The data show that the estimated slope under these conditions can be less than that predicted by probability summation (-0.20), which in turn may be taken as apparent evidence against global summation (Mullen et al., 2011). Data in all plots are the average of three observers. Error bars are standard errors of the means.

pooling reported by Mullen, Beaudot, and Ivanov (2011). Given this scale and shape invariant behavior, we conducted the following experiments with small RF5 patterns with high spatial frequencies, in order for the results to be comparable to the other conditions tested in our study.

Secondly, presentation time can be ruled out as increasing presentation time has a negligible effect on performance (Fig. 6C) and the slopes for both the short (160 ms) and long (1000 ms) presentation time indicate global processing.

Thirdly, Mullen and colleagues used a different way to isolate fractions of an RF contour compared to ours. Their aperture was composed of a single Gaussian function defining the contrast along the contour's circumference. We found no difference when substituting our method (displaying a full, unaltered cycle of an

RF and rapidly decreasing the contrast on each side of it) with that employed by Mullen, Beaudot, and Ivanov (2011). Both methods give similar results (data not shown), for high and low contrasts, and consequently are both consistent with global pooling. Hence, differences in the details of the windowing functions cannot explain the differences between the two studies.

Finally, we find that contrast does have a substantial effect on sensitivity to shape discrimination (Fig. 6D). Lowering the contrast of the stimuli to five times the contrast detection threshold of a circle (open squares) increases thresholds by about a factor of 2 (compared to the high contrast condition shown by the open diamonds). Importantly, reducing the contrast decreases sensitivity for isolated cycles and entire contours by similar amounts. Thus, the strength of integration, measured as the slope of the line

connecting these two points, is similar (−0.61 for 100% contrast; −0.51 for contrasts of five times the detection threshold; Fig. 6D). Hence, evidence for global pooling that exceeds the prediction of probability summation is seen when both an isolated cycle and a complete contour have high or low contrasts. Given that contrast alters sensitivity for both an isolated cycle and a complete contour, the apparent strength of integration (i.e. comparing performance for a single cycle with that for the entire contour) *will* change when different contrast values are used for a single cycle and the entire contour. In Mullen et al.'s study, patterns were typically presented at the same level of *visibility* (at five times their respective contrast detection thresholds). Because the contrast detection threshold is higher for a single cycle compared to an entire closed contour, this results in different absolute contrasts for single cycles and entire contours. Consequently, the measured slopes (integration strengths) apparently decrease because the contrast for the single cycle is higher (and thereby yielding a lower shape discrimination threshold) than that for the entire contour. Our data (Fig. 6D) show that the estimated slope under these mixed contrast conditions can be less than that predicted by probability summation (−0.20), which, in turn, may be taken as apparent evidence against global summation. In Fig. 3D of Mullen, Beaudot, and Ivanov (2011), the data for one of the observers (KTM) are fitted by a line with a slope that we estimate to be approximately −0.16, which is in the same range as we report here. However, it is of note that the figure in Mullen, Beaudot, and Ivanov (2011) shows data plotted on lin–log axes, whereas we always show data on log–log axes, making direct visual comparison of the line slopes difficult. Even data following the behavior of perfect linear pooling would appear to exhibit a shallow relationship between number of cycles (in linear coordinates) and thresholds (log). Comparison of the data in Mullen et al.'s Fig. 3 with the prediction for probability summation is also difficult. The prediction is shown in their Fig. 3 as straight lines, but any power-law relationship such as probability summation only falls on straight lines when plotted in log–log coordinates. In lin–log coordinates, that prediction should follow a curved line. Moreover, differences between experimental data and the prediction made by probability summation are over-emphasized in Fig. 3 (C and D) of Mullen, Beaudot, and Ivanov (2011): we have estimated that the slope of the lines depicting probability summation is approximately −1.66 rather than −0.33.

In summary, we confirm and extend a number of previous investigations (Bell & Badcock, 2008, 2009; Habak, Wilkinson, & Wilson, 2006; Hess, Wang, & Dakin, 1999; Jeffrey, Wang, & Birch, 2002; Loffler, Wilson, & Wilkinson, 2003; Wilkinson, Wilson, & Habak, 1998), which have reported evidence in favor of global pooling underlying the high sensitivity of human observers when discriminating RF patterns. The presence of global pooling, as well as its strength, is largely independent of pattern shape, size, presentation time and absolute contrast and seen for low pattern amplitudes (discrimination against a circle) as well as high amplitudes. Situations in which global pooling is not evident include partially modulated contours and shapes with sufficiently high numbers of lobes (high radial frequency).

4. Discussion

The aim of the current study was to investigate and compare the strength of global pooling for a variety of circular and non-circular shapes. Sensitivity for RF shape discrimination has been shown to be in the hyperacuity range (Loffler, Wilson, & Wilkinson, 2003; Wilkinson, Wilson, & Habak, 1998). These earlier studies were concerned with discrimination of RF patterns against circles and therefore only tested a limited range of quasi-circular shapes.

Our results show that subjects' performance remains in the hyperacuity range for various non-circular shapes (Figs. 2, 3 and 5): for RF3 up to and including amplitudes of 2.5× detection threshold, for RF5 up to 5×, and up to 10× for RF20.

4.1. Strength of global pooling for circular and non-circular shapes

Global pooling has previously been reported to underlie the high sensitivity for the discrimination of RF patterns from circles (Bell & Badcock, 2008, 2009; Habak, Wilkinson, & Wilson, 2006; Hess, Wang, & Dakin, 1999; Jeffrey, Wang, & Birch, 2002; Loffler, Wilson, & Wilkinson, 2003; Wilkinson, Wilson, & Habak, 1998). To compare the strength of this pooling for a variety of shapes, we investigated a range of non-circular stimuli. Sensitivities were compared when various fractions of the contours were modulated. Analogous to the analysis in Loffler, Wilson, and Wilkinson (2003), we have considered there to be evidence in favor of a global mechanism when the increase in sensitivity with increasing number of modulated cycles exceeds the prediction of probability summation over independent local detectors. In contrast to the study of Loffler, Wilson, and Wilkinson (2003), where the improvement in performance with increasing number of modulated cycles followed a power-law (linear relationship in log–log coordinates), our data for low RFs (3 and 5) are not well captured by this relationship. Instead, we see a non-linear relationship with a modest increase in sensitivity with increasing numbers of modulated cycles up to but excluding the point where the entire pattern is modulated. Sensitivity when the entire pattern is modulated is substantially higher than that when a small part stays unmodulated. Accordingly, two regimes can be identified, a shallow part ranging from 1 to 2 cycles for RF3 and 1 to 4 cycles for RF5 and a steep part for the 'pure' RF patterns. A linear curve (power-law) fit cannot accurately describe the consistent "knee-shaped" characteristic of our data. Instead, a two-line fit is required. The average slopes (−0.20 for RF3 and −0.32 for RF5) of the shallow regime are in the range of probability summation (−0.33). This is evident for shapes with low and high amplitudes (Figs. 2–4). To quantify the amount of global pooling, we calculated the improvement in performance between a shape with one modulated cycle and a fully modulated pattern. The results consistently exceed the prediction of probability summation in all tested conditions (average slopes across RF3 and RF5 = −0.60), arguing for a global mechanism underlying RF discrimination, but only if the entire pattern is deformed. The characteristic gradual increase in performance between 1 and 2 cycles for RF3 and from 1 to 4 cycles for RF5 and the marked increase in performance as the entire pattern is manipulated argues in favor of highly specialized, non-linear shape mechanisms.

A possible reconciliation of the linear relationship reported in earlier studies (Loffler, Wilson, & Wilkinson, 2003) with the two regimes seen here is that in the previous investigation they sampled the number of modulated cycles more sparsely than here. That study only tested 1 and 3 cycles of an RF3 and 1, 3 and 5 cycles of an RF5. As can be appreciated from Fig. 3A, data points for 1, 3 and 5 cycles of an RF5 can be fit reasonably well by a straight line. However, across all conditions straight lines provide a poor fit. Omitting the intermediate cycles is therefore a possible explanation for why only a simple power-law relationship was observed before.

4.2. Factors affecting global pooling

Global pooling underlying RF discrimination has not always been reported. In contrast to the global pooling seen in our data as well as in many previous studies (Bell & Badcock, 2008, 2009; Habak, Wilkinson, & Wilson, 2006; Hess, Wang, & Dakin, 1999;

Jeffrey, Wang, & Birch, 2002; Loffler, Wilson, & Wilkinson, 2003; Wilkinson, Wilson, & Habak, 1998), Mullen, Beaudot, and Ivanov (2011) recently reported only marginal, insignificant improvements in discrimination ability when comparing performance for an isolated cycle of a low contrast RF4 to that of a complete RF4 pattern. This was interpreted as evidence against global pooling. The authors suggest that when observers are confronted with a closed contour where only a part of it is modulated, with the remainder staying constant (e.g. circular), attentional effects might influence performance. The presence of the task irrelevant remaining contour (which was used in many of the previous studies and in our Experiment 1) is argued to be responsible for the comparatively poor performance for single modulated cycles and the consequently observed superiority of fully modulated patterns. This attentional impairment might not affect, or might affect to a lesser extent, a condition with a single, isolated RF cycle. This explanation is, however, inconsistent with results from previous studies (Loffler, Wilson, & Wilkinson, 2003). Introducing spatial certainty by fixing the orientation of the contour (and therefore the position of the modulated part) should eliminate attentional effects by abolishing spatial uncertainty with respect to the specific location where the pattern is deformed. One would then predict that performance for a single cycle, as part of a closed contour, should improve to a level comparable to that for a pure RF. This is contrary to what we (data not shown), as well as others (Loffler, Wilson, & Wilkinson, 2003), have found. Performance for one modulated cycle at a fixed location as part of a closed contour is much poorer than for a fully modulated RF. Hence, evidence for global summation is still seen in circumstances of spatial certainty.

According to signal detection theory (Green & Swets, 1966; Petrov, Verghese, & McKee, 2006) the elimination of spatial uncertainty (e.g. fixing the orientation of the contour and thus the position of the modulated part) should also result in a steeper slope of the psychometric functions. In our experiments the slopes of the psychometric functions are largely independent of the absence or presence of spatial certainty (slopes ranging between 2.5 and 3.0). This argues against spatial uncertainty playing a major role in this type of shape discrimination. Hence, our results do not show attention to be responsible for the poorer performance for single modulated cycles of an otherwise unmodulated contour compared to thresholds reached with patterns that are modulated everywhere.

Mullen, Beaudot, and Ivanov (2011) also argue that the poorer performance for single modulated cycles in previous studies (Hess, Wang, & Dakin, 1999; Loffler, Wilson, & Wilkinson, 2003) might result from the missing information around the points of zero-crossing (inflection points). Their data show a rapid increase in performance up to 1 cycle and a subsequent plateau with performance largely unaffected by increasing the number of cycles. We have not tested less than 1 cycle but unlike the earlier study with isolated segments, we do see a significant improvement in sensitivity when comparing one deformed cycle with a completely deformed contour.

We investigated a number of potential factors that might explain why global summation was not observed in Mullen et al.'s study. We find integration strength (measured as the slope of the line connecting the sensitivity for a single, isolated cycle to that of an entire modulated RF) to be above the level predicted by probability summation and hence consistent with global pooling for changes in pattern shape, scale (i.e. change in size and contour spatial frequency) and presentation time. All these represent differences between our initial experiment and those of Mullen, Beaudot, and Ivanov (2011) and we conclude that none of these can explain the discrepancies.

Our data show that contrast has a substantial effect on the overall sensitivity to shape discrimination. Reducing the contrast decreases sensitivity for isolated cycles and entire contours by similar amounts. The same strength of integration, measured as the slope of the line connecting these two points, is seen for high and low contrasts. However, the apparent strength of integration *will* change when different contrast values are used for a single cycle and the entire contour as in Mullen, Beaudot, and Ivanov's (2011) study. Our data show that the estimated slope under these mixed contrast conditions can be less than that predicted by probability summation. This provides an explanation for the discrepancies between studies and shows that presenting stimuli at the same level of visibility, by adjusting contrasts independently for different stimuli, underestimates the strength of global integration for RF discrimination.

After this manuscript had been submitted, a study (Ivanov & Mullen, 2012) was published, which also investigated the role of contrast on RF shape discrimination. The results from the two studies agree in that sensitivity depends on stimulus contrast: lowering contrast from 100% to as low as 5× detection threshold increases thresholds by a factor of about 2 to 3. While Ivanov and Mullen only investigated fully modulated RF contours, our data show that contrast has a similar effect on the overall sensitivity for isolated cycles as well as entire contours.

While there are situations in which it will be desirable to equate stimuli according to their individual visibility (e.g. when comparing the effects of chromatic and achromatic patterns), we argue that the same absolute contrast should be used for 1 cycle and an entire pattern when determining integration strength. Given that overall sensitivity depends on absolute contrast, employing different contrasts for different stimuli (1 cycle vs. many cycles) will result in a level of performance that depends on two factors, the number of cycles as well as contrast. If one aims to investigate the integration strength of a putative mechanism that has access to information across extended contours, its performance should be compared when all parameters but the contour length are fixed, including contrast. This approach has been taken in a variety of experiments, which aimed to investigate the effect of stimulus extent on observer sensitivity (e.g. Bell & Badcock, 2008; Hess, Wang, & Dakin, 1999; Loffler, Wilson, & Wilkinson, 2003; Morrone, Burr, & Vaina, 1995; Wilson & Wilkinson, 1998; Wilson, Wilkinson, & Asaad, 1997). For low as well as high contrast RF patterns, if contrast is fixed in this fashion, the integration strength is in excess of probability summation and therefore consistent with global pooling.

While this explains why Mullen et al. did not find evidence for global summation in most of their experiments, it remains unclear why they did not find global summation in a control condition (on a small number of observers) with the same absolute contrast for a single cycle and the entire contour.

A separate issue concerns what difference in slopes might be expected when comparing the situation where more and more of a contour is made visible to that where more and more of an entirely visible contour is modulated (Fig. 6A). As discussed in the results for Experiment 2, we observed slopes of approximately −0.6 in both cases. This cannot be fully explained by a simple linear pooling model, which would predict a slope of −0.5 in the former case and a slope of −1.0 in the latter (Morrone, Burr, & Vaina, 1995). In this simple model, increasing the number of visible cycles increases the number of early stage units integrated by a global integrator while increasing the amount of contour modulation does not affect the number of integrated units. Assuming noisy input units, the slope in the former case (noise and signal both increase) would be −0.5, while in the latter case (only signal increases with constant noise) it would be −1.0 (Morrone, Burr, & Vaina, 1995).

An alternative model might place the limiting noise at a late stage where signal integration takes place. In this case, the slope
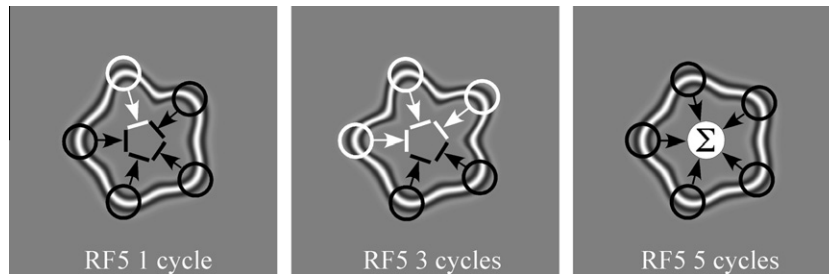
Fig. 7. Qualitative model for RF pattern discrimination. The right image shows a pure RF5 pattern (i.e. all cycles are equally modulated). The information from multiple local detectors, indicated by the black rings (for example curvature detectors centered at the contour's maximum curvature), is integrated (Σ) by a pooling mechanism, if all detectors deliver an identical signal (right). If, however, the local signals differ (indicated by the white rings) as for the RF5 with 1 modulated cycle (left) and 3 modulated cycles (center), the global summation mechanism is not activated (black bars). As a result, sensitivity in these cases is limited by the probabilistic summation of local information, rather than the more efficient global pooling. As a consequence, discrimination performance as a function of modulated cycles increases marginally from 1 to 1 cycle less than the entire contour but shows a drastic improvement when the entire contour is modulated.

for both conditions would be the same: −1.0 (Heeley & Buchanan-Smith, 1996; Morgan, Ward, & Hole, 1990). The same prediction would be reached under the assumption of early noise and obligatory pooling (Parkes et al., 2001; Wilson & Wilkinson, 1998).

While our data cannot unequivocally distinguish between these models, the similar integration slopes for isolated vs. partially modulated contours favors the latter models. In any case, it is clear that the measured slopes of more than −0.33 but less than −1.0 are indicative of global pooling mechanisms that operate less efficiently than a perfect linear integrator.

A final remark concerns differences in task difficulty for different shapes. It may be argued that the task of discriminating two RF contours at non-zero amplitudes (e.g. two star-shaped patterns) may be more difficult than one where observers have to discriminate a circle from a (just noticeable) non-circular shape. The higher thresholds for the non-zero amplitude patterns might be explained by this possibility. However, it is clear that any such task-related difference does not affect the overall observation of global pooling: evidence for global summation is present, and indeed similar, for the discrimination of circular and e.g. star-shaped contours.

4.3. Implications for contour shape computation

The common pattern of our results from Experiment 1 is that discrimination thresholds decrease according to the prediction of probability summation up to, but not including, the point where the pattern is modulated in its entirety. This argues in favor of a highly specialized shape processing mechanism, which is only activated when the entire pattern is deformed. If only fractions are manipulated, data are consistent with performance limited by local processes.

The presence of two regimes is reminiscent of results from investigations into motion perception. Morrone, Burr, and Vaina (1995) measured direction discrimination thresholds and contrast sensitivity for radial, circular and translational motion of Gaussian patches, where various numbers of "sectors" of the stimulus display were exposed. The aim of these experiments was to examine the integration properties of motion information across space. Data were consistent with the existence of ideal, linear integrators summing local motion signals over extended regions. When measuring the summation of contrast sensitivity, direction discrimination for radial motion dramatically increased with increasing number of presented sectors until a certain stage after which performance improved only slightly. The authors suggested that the first part of the increase in discrimination ability reflects linear summation (physiological summation) whereas the second part is due to information from multiple, independent local mechanisms being combined by probability summation.

We have not tested signal integration for very small amounts of RF contours (less than 1 cycle) but results from previous studies show strong signal integration up to 1 cycle for low (Mullen, Beaudot, & Ivanov, 2011) and high contrast RF segments (Loffler, Wilson, & Wilkinson, 2003). Combined with our results, it appears that processing of RF patterns shows three distinct regimes of signal integration: strong summation up to about 1 cycle, little summation between 1 cycle and 1 cycle less than a complete RF (e.g. RF5 with 4 modulated cycles) and strong summation for complete RFs.

Based on this and our results presented here, we propose that RF sensitivity might be explained by a three-stage process. At the first stage, information is processed by local detectors tuned to contour parts and the strong summation within 1 cycle is evidence of the physiological integration at this stage. At the second stage, information from multiple independent local detectors is compared and performance predicted by probability summation. At the third stage, the information from local detectors is integrated by another physiological mechanism, resulting in a rapid increase in sensitivity.

Fig. 7 illustrates a simple model that can qualitatively predict our data. The model assumes a global integration (summation) mechanism, which is only activated when it is stimulated simultaneously by identical local signals. This computation could be realized by an 'and' gate although this is only one of a number of possible ways in which the outputs from local units (e.g. curvature detectors) may be integrated. Other alternatives include cross-correlation (as employed in physiologically plausible motion detectors: van Santen & Sperling, 1985) or multiplication (evidence for which has been reported for the processing of contour segments: Gheorghiu & Kingdom, 2009). Our data do not allow us to distinguish between these possibilities although they indicate the presence of a non-linear mechanism of such a type that is only active when presented with patterns with matched local properties (e.g. curvature).

The local detectors that provide the input to the global mechanism could originate from a set of putative curvature detectors in V1 or V2 (Dobbins et al., 1987, 1989; Koenderink & Richards, 1988; Wilson, 1985; Wilson & Richards, 1989), with receptive fields centered at different points along the contour's circumference. Psychophysical evidence for RF discrimination exists in favor of models based on such units centered at points of maximum curvature (Bell et al., 2008; Habak et al., 2004; Loffler, Wilson, & Wilkinson, 2003; Poirier & Wilson, 2006, 2007; Poirier & Wilson, 2010), inflections (Hess, Wang, & Dakin, 1999; Kurki, Saarinen, & Hyvarinen, 2009; Mullen & Beaudot, 2002) or a combination of the two (Bell et al., 2010). The global summation stage is hypothesized to occur in V4, using responses from matched curvature

units, for which there is physiological evidence in macaque (Gallant, Braun, & Van Essen, 1993) and humans (Wilkinson et al., 2000). The predictions from this model are based on comparing the outputs from multiple independent curvature detectors via probability summation unless the entire pattern is modulated. Only then is the 'physiological' pooling stage activated, resulting in the increase in sensitivity that is evident from our data. In a 2AFC experiment, maximum sensitivity results when both test and reference patterns activate the global mechanism. If only a fraction of the contour is modulated, the summation mechanism stays silent. Hence, subjects are always better at discriminating two 'pure' RF patterns (e.g. circle from RF5) than when one of the patterns is partially modulated.

It has previously been suggested that global pooling for RF patterns only extends up to frequencies of about 10 and is not evident for higher radial frequencies (Loffler, Wilson, & Wilkinson, 2003). In one condition, we tested discrimination thresholds for an RF20 (Fig. 4) to investigate how spatial pooling depends on radial frequency. As for low RFs, for an RF20 the thresholds decrease with increasing number of modulated cycles but, unlike low RFs, this decrease is well described by a *single* power-law relationship. The two regimes seen for low RFs are not evident for higher RFs. The increase in performance for RF20 is in the range of probability summation, which is in accord with previous results (Loffler, Wilson, & Wilkinson, 2003). Loffler et al. argued that such higher frequency patterns are not processed by special mechanisms pooling information across the entire contour. Rather, performance for these patterns is limited by probability summation over local, independent channels.

What could be the ecological advantage for developing cortical networks that are tuned to pure but not partial RFs? One advantage of pure RF detectors is that these shapes could be used as a base set to describe more complex shapes. According to the 'Fourier descriptor' proposal (Alter & Schwartz, 1988; Zahn & Roskies, 1972) any complex two-dimensional closed contour can be described by a sum of elementary components. Pure RFs are one such set of components (Wilkinson, Wilson, & Habak, 1998) and may play a fundamental role in complex shape description. Future studies are required to address this possibility.

Pure RF patterns are symmetrical. Depending on the radial frequency, pure RF patterns have various axes of symmetry (e.g. an RF5 has 5 symmetry axes). Previous research has revealed that humans are remarkably sensitive to mirror symmetric objects, especially for those with vertical axes of symmetry (Barlow & Reeves, 1979; Wagemans, Van Gool, & d'Ydewalle, 1992; Wenderoth, 1994). Furthermore, it was shown that discrimination between asymmetric and symmetric shapes is very fast and requires no more than 25 ms (Carmody, Nodine, & Locher, 1977). Applied to RFs, one might predict that performance for discriminating pure symmetric RF patterns from partly modulated RFs, which have no symmetry axes, would be better than when both patterns are symmetric. Our results show the opposite effect. For RF discrimination, subjects are substantially better in discriminating two contours that are symmetric than between two patterns where one is symmetric and the other is not. This discrepancy is a matter for future investigations.

In summary, our data for a variety of RFs (3 and 5) with a range of modulation amplitudes show a moderate increase in discrimination ability with an increasing number of modulated cycles, which is well captured by probability summation. This is, however, only seen when fractions of the contour are modulated. As soon as the entire contour is modulated, performance improves dramatically. This cannot be explained by local computations and instead requires global integration. The non-linearity of the dependence of sensitivity on the amount of deformed contour argues in favor of a highly specialized shape mechanism that is active only when the entire pattern is modulated.

References

Alter, I., & Schwartz, E. L. (1988). Psychophysical studies of shape with Fourier descriptor stimuli. *Perception, 17*(2), 191–202.

Anderson, N. D., Habak, C., Wilkinson, F., & Wilson, H. R. (2007). Evaluating shape after-effects with radial frequency patterns. *Vision Research, 47*(3), 298–308.

Anzai, A., Peng, X., & Van Essen, D. C. (2007). Neurons in monkey visual area V2 encode combinations of orientations. *Nature Neuroscience, 10*(10), 1313–1321.

Barlow, H. B., & Reeves, B. C. (1979). The versatility and absolute efficiency of detecting mirror symmetry in random dot displays. *Vision Research, 19*(7), 783–793.

Bell, J., & Badcock, D. R. (2008). Luminance and contrast cues are integrated in global shape detection with contours. *Vision Research, 48*(21), 2336–2344.

Bell, J., & Badcock, D. R. (2009). Narrow-band radial frequency shape channels revealed by sub-threshold summation. *Vision Research, 49*(8), 843–850.

Bell, J., Badcock, D. R., Wilson, H., & Wilkinson, F. (2007). Detection of shape in radial frequency contours: Independence of local and global form information. *Vision Research, 47*(11), 1518–1522.

Bell, J., Dickinson, J. E., & Badcock, D. R. (2008). Radial frequency adaptation suggests polar-based coding of local shape cues. *Vision Research, 48*(21), 2293–2301.

Bell, J., Hancock, S., Kingdom, F. A., & Peirce, J. W. (2010). Global shape processing: Which parts form the whole? *Journal of Vision, 10*(6), 1–13.

Bell, J., Wilkinson, F., Wilson, H. R., Loffler, G., & Badcock, D. R. (2009). Radial frequency adaptation reveals interacting contour shape channels. *Vision Research, 49*(18), 2306–2317.

Brainard, D. H. (1997). The psychophysics toolbox. *Spatial Vision, 10*(4), 433–436.

Carmody, D. P., Nodine, C. F., & Locher, P. J. (1977). Global detection of symmetry. *Perceptual and Motor Skills, 45*(3 Pt 2), 1267–1273.

Connor, C. E., Brincat, S. L., & Pasupathy, A. (2007). Transformation of shape information in the ventral pathway. *Current Opinion in Neurobiology, 17*(2), 140–147.

Dobbins, A., Zucker, S. W., & Cynader, M. S. (1987). Endstopped neurons in the visual cortex as a substrate for calculating curvature. *Nature, 329*(6138), 438–441.

Dobbins, A., Zucker, S. W., & Cynader, M. S. (1989). Endstopping and curvature. *Vision Research, 29*(10), 1371–1387.

Dumoulin, S. O., & Hess, R. F. (2007). Cortical specialization for concentric shape processing. *Vision Research, 47*(12), 1608–1613.

Gallant, J. L., Braun, J., & Van Essen, D. C. (1993). Selectivity for polar, hyperbolic, and Cartesian gratings in macaque visual cortex. *Science, 259*(5091), 100–103.

Gallant, J. L., Connor, C. E., Rakshit, S., Lewis, J. W., & Van Essen, D. C. (1996). Neural responses to polar, hyperbolic, and Cartesian gratings in area V4 of the macaque monkey. *Journal of Neurophysiology, 76*(4), 2718–2739.

Gheorghiu, E., & Kingdom, F. A. (2009). Multiplication in curvature processing. *Journal of Vision, 9*(2), 23, 21–17.

Goodale, M. A., & Milner, A. D. (1992). Separate visual pathways for perception and action. *Trends in Neurosciences, 15*(1), 20–25.

Graham, N. (1989). *Visual pattern analyzers.* New York: Oxford University Press.

Graham, N., & Robson, J. G. (1987). Summation of very close spatial frequencies: The importance of spatial probability summation. *Vision Research, 27*(11), 1997–2007.

Green, D. M., & Swets, J. A. (1966). *Signal detection theory and psychophysics.* New York: Wiley.

Gross, C. G. (2008). Single neuron studies of inferior temporal cortex. *Neuropsychologia, 46*(3), 841–852.

Habak, C., Wilkinson, F., & Wilson, H. R. (2006). Dynamics of shape interaction in human vision. *Vision Research, 46*(26), 4305–4320.

Habak, C., Wilkinson, F., Zakher, B., & Wilson, H. R. (2004). Curvature population coding for complex shapes in human vision. *Vision Research, 44*(24), 2815–2823.

Heeley, D. W., & Buchanan-Smith, H. M. (1996). Mechanisms specialized for the perception of image geometry. *Vision Research, 36*(22), 3607–3627.

Hegde, J., & Van Essen, D. C. (2000). Selectivity for complex shapes in primate visual area V2. *Journal of Neuroscience, 20*(5), RC61.

Hess, R. F., Achtman, R. L., & Wang, Y. Z. (2001). Detection of contrast-defined shape. *Journal of the Optical Society of America A: Optics, Image Science, and Vision, 18*(9), 2220–2227.

Hess, R. F., Wang, Y. Z., & Dakin, S. C. (1999). Are judgements of circularity local or global? *Vision Research, 39*(26), 4354–4360.

Hubel, D. H., & Wiesel, T. N. (1962). Receptive fields, binocular interaction and functional architecture in the cat's visual cortex. *Journal of Physiology, 160*, 106–154.

Hubel, D. H., & Wiesel, T. N. (1968). Receptive fields and functional architecture of monkey striate cortex. *Journal of Physiology, 195*(1), 215–243.

Ito, M., Fujita, I., Tamura, H., & Tanaka, K. (1994). Processing of contrast polarity of visual images in inferotemporal cortex of the macaque monkey. *Cerebral Cortex, 4*(5), 499–508.

Ivanov, I. V., & Mullen, K. T. (2012). The role of local features in shape discrimination of contour- and surface-defined radial frequency patterns at low contrast. *Vision Research, 52*(1), 1–10.

Jeffrey, B. G., Wang, Y. Z., & Birch, E. E. (2002). Circular contour frequency in shape discrimination. *Vision Research, 42*(25), 2773–2779.

　　　　　　　　　　　　　　　　　　　　　　　　　　　　　　G. Schmidtmann et al. / Vision Research 62 (2012) 44–56

Koenderink, J. J., & Richards, W. A. (1988). Two-dimensional curvature operators. *Journal of the Optical Society of America A: Optics, Image Science, and Vision, 5*(7), 1136–1141.

Kurki, I., Saarinen, J., & Hyvarinen, A. (2009). Integration of contour features into a global shape: A classification image study. *Perception, 38* (Abstract Supplement 25).

Loffler, G. (2008). Perception of contours and shapes: Low and intermediate stage mechanisms. *Vision Research, 48*, 2106–2127.

Loffler, G., Wilson, H. R., & Wilkinson, F. (2003). Local and global contributions to shape discrimination. *Vision Research, 43*(5), 519–530.

Missal, M., Vogels, R., Li, C. Y., & Orban, G. A. (1999). Shape interactions in macaque inferior temporal neurons. *Journal of Neurophysiology, 82*(1), 131–142.

Morgan, M. J., Ward, R. M., & Hole, G. J. (1990). Evidence for positional coding in hyperacuity. *Journal of the Optical Society of America A: Optics, Image Science, and Vision, 7*(2), 297–304.

Morrone, M. C., Burr, D. C., & Vaina, L. M. (1995). Two stages of visual processing for radial and circular motion. *Nature, 376*(6540), 507–509.

Mullen, K. T., & Beaudot, W. H. (2002). Comparison of color and luminance vision on a global shape discrimination task. *Vision Research, 42*(5), 565–575.

Mullen, K. T., Beaudot, W. H., & Ivanov, I. V. (2011). Evidence that global processing does not limit thresholds for RF shape discrimination. *Journal of Vision, 11*(3), 1–21.

Murray, S. O., Kersten, D., Olshausen, B. A., Schrater, P., & Woods, D. L. (2002). Shape perception reduces activity in human primary visual cortex. *Proceedings of the National Academy of Sciences of the United States of America, 99*(23), 15164–15169.

Ohla, K., Busch, N. A., Dahlem, M. A., & Herrmann, C. S. (2005). Circles are different: The perception of Glass patterns modulates early event-related potentials. *Vision Research, 45*(20), 2668–2676.

Parkes, L., Lund, J., Angelucci, A., Solomon, J. A., & Morgan, M. (2001). Compulsory averaging of crowded orientation signals in human vision. *Nature Neuroscience, 4*(7), 739–744.

Pasupathy, A., & Connor, C. E. (1999). Responses to contour features in macaque area V4. *Journal of Neurophysiology, 82*(5), 2490–2502.

Pasupathy, A., & Connor, C. E. (2001). Shape representation in area V4: Position-specific tuning for boundary conformation. *Journal of Neurophysiology, 86*(5), 2505–2519.

Pasupathy, A., & Connor, C. E. (2002). Population coding of shape in area V4. *Nature Neuroscience, 5*(12), 1332–1338.

Pelli, D. G. (1997). The VideoToolbox software for visual psychophysics: Transforming numbers into movies. *Spatial Vision, 10*(4), 437–442.

Petrov, Y., Verghese, P., & McKee, S. P. (2006). Collinear facilitation is largely uncertainty reduction. *Journal of Vision, 6*(2), 170–178.

Poirier, F. J. A. M., & Wilson, H. R. (2010). A biologically plausible model of human shape symmetry perception. Journal of Vision, 10(1):9, 1–16.

Poirier, F. J. A. M., & Wilson, H. R. (2006). A biologically plausible model of human radial frequency perception. *Vision Research, 46*, 2443–2455.

Poirier, F. J., & Wilson, H. R. (2007). Object perception and masking: Contributions of sides and convexities. *Vision Research, 47*(23), 3001–3011.

Quick, R. F. Jr., (1974). A vector-magnitude model of contrast detection. *Kybernetik, 16*(2), 65–67.

Tanaka, K. (1996). Inferotemporal cortex and object vision. *Annual Review of Neuroscience, 19*, 109–139.

Ungerleider, L. G., & Mishkin, M. (1982). Two cortical visual systems. In D. J. Ingle & M. A. Goodale (Eds.), *Analysis of visual behavior* (pp. 549–586). Cambridge: MIT Press.

van Santen, J. P., & Sperling, G. (1985). Elaborated Reichardt detectors. *Journal of the Optical Society of America A: Optics, Image Science, and Vision, 2*(2), 300–321.

Wagemans, J., Van Gool, L., & d'Ydewalle, G. (1992). Orientational effects and component processes in symmetry detection. *The Quarterly Journal of Experimental Psychology, 44*(A), 475–508.

Wenderoth, P. (1994). The salience of vertical symmetry. *Perception, 23*(2), 221–236.

Westheimer, G. (1979). The spatial sense of the eye. Proctor lecture. *Investigative Ophthalmology & Visual Science, 18*(9), 893–912.

Wilkinson, F., James, T. W., Wilson, H. R., Gati, J. S., Menon, R. S., & Goodale, M. A. (2000). An fMRI study of the selective activation of human extrastriate form vision areas by radial and concentric gratings. *Current Biology, 10*(22), 1455–1458.

Wilkinson, F., Wilson, H. R., & Habak, C. (1998). Detection and recognition of radial frequency patterns. *Vision Research, 38*(22), 3555–3568.

Wilson, H. R. (1985). Discrimination of contour curvature: Data and theory. *Journal of the Optical Society of America A: Optics, Image Science, and Vision, 2*(7), 1191–1199.

Wilson, H. R., & Richards, W. A. (1989). Mechanisms of contour curvature discrimination. *Journal of the Optical Society of America A: Optics, Image Science, and Vision, 6*(1), 106–115.

Wilson, H. R., & Wilkinson, F. (1998). Detection of global structure in Glass patterns: Implications for form vision. *Vision Research, 38*(19), 2933–2947.

Wilson, H. R., Wilkinson, F., & Asaad, W. (1997). Concentric orientation summation in human form vision. *Vision Research, 37*(17), 2325–2330.

Zahn, C. T., & Roskies, R. Z. (1972). Fourier descriptors for plane closed curves. *IEEE Transactions on Computers, 21*, 269–281.